

AUTOMATIC FILTER DESIGN IN HARP ANALYSIS OF TAGGED MAGNETIC RESONANCE IMAGES

M. Marinelli^{1,2}, V. Positano², N.F. Osman³, F.A. Recchia¹, M. Lombardi², L. Landini⁴

¹Scuola Superiore Sant'Anna, Pisa, Italy, ²MRI Lab, CNR Institute of Clinical Physiology, Pisa, Italy
³JHU, Baltimore, USA, ⁴Dep. of Information Engineering, University of Pisa, Pisa, Italy

ABSTRACT

Harmonic phase (HARP) is an image processing technique of MR-tagged images in frequency domain developed to evaluate the regional tissue strain. The filtering stage is a key point in this method because all information about the deformation have to be included in the analysis. In this paper we develop an automatic method to define the filter parameters in order to minimize errors in the strain evaluation and to avoid operator related variability. A software model is built to investigate the error in strain estimation caused by filter parameters variability and to evaluate the developed method. The automatic technique models each spectral peak with a bidimensional Gaussian function and uses these information to create an optimal elliptic filter. We validated the automatic method on simulated data set. In real tagged MR images analysis, the method achieved the same performance as the manual analysis, considered the gold standard, eliminating the inter-operator variability.

Index Terms— Automatic filter, image processing, magnetic resonance tagging, strain analysis, software model.

1. INTRODUCTION

Magnetic resonance tagging is a useful and noninvasive technique to evaluate the regional tissue motion and strain [1] in normal and abnormal myocardium. Although the image acquisition method has achieved good performance, the time-consuming postprocessing has limited the tagging analysis in clinical routine.

Harmonic phase technique (HARP) [2][3] has been developed to overcome the principal limits of image analysis. It is based on the fact that SPAMM-tagged MR images produce an array of spectral peaks in the Fourier domain and each spectral peak carries information about the motion in a certain direction. The inverse Fourier transform of each individual peak, extracted using a bandpass filter, is a complex image whose phase is linearly related to a directional component of the motion [4]. The filtering step is a key point in the HARP method. In the original form, this technique uses a filter with a constant elliptical bandpass region and a Gaussian rolloff outside [5]. The most important parameter of this filter is the

cut-off frequency. Indeed, the cardiac deformation causes the changes in the Fourier spectrum of each acquired image [6]. From diastole to systole, the spectral peaks move away from the origin and their size increases [5]. Therefore a too narrow filter suppresses the tag modulation in areas with large deformation, whereas a too wide filter introduces artifacts in the strain evaluation.

In this paper, we propose an automatic method to define the elliptical filter parameters for including in the filtered images all information about the cardiac deformation, and excluding other information that can introduce a large error in the strain evaluation. We build a software model to simulate the MR-tagged images. We use this model to investigate the error in strain estimation caused by filter parameters variability and to evaluate the developed algorithm. Finally, we compare on real data the strain results obtained using both the manual and the automatic method for elliptical filter parameters definition.

2. MATERIALS AND METHODS

2.1. Phantom

We simulated SPAMM tagged images of a deforming and incompressible cylinder [7][8][9] such that a material point (R, Θ, Z) in the undeformed state displaces to (r, ϑ, z) in the deformed state as the following equation:

$$\begin{aligned} r &= r(R) & \vartheta &= \phi R + \Theta + \gamma Z + \epsilon \\ z &= \omega R + \lambda Z + \delta \end{aligned} \quad (1)$$

Due to incompressibility, the function $r(R)$ is given by:

$$r(R) = \sqrt{r_i^2 + \frac{1}{\lambda}(R^2 - R_i^2)} \quad (2)$$

where R_i and r_i are the inner radii of the cylinder before and after deformation. The kinematic parameters were chosen similar to [7][8][9] to exaggerate the motion of the human heart: $R - \Theta$ shear $\phi = 0.556^\circ/\text{mm}$, rigid body rotation $\epsilon = 9.2^\circ$, longitudinal contraction $\lambda = 1$, axial torsion $\gamma = 0.6^\circ/\text{mm}$, $R - Z$ shear $\omega = 0.248$ and rigid body displacement $\delta = 4.167$ mm. In the undeformed state, at time

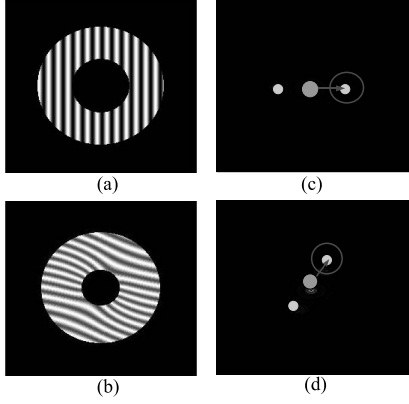


Fig. 1. Simulated SPAMM tagged images of the first (a) and last frame (b) and their schematic Fourier transform images in (c) and (d) respectively.

phase 0, the cylinder has an inner radius $R_i = 15$ mm, an outer radius $R_o = 33$ mm and a length $Z = 100$ mm. To simulate short axis images, imaging planes were defined at $z = 20, 30, 40, 50, 60, 70, 80$ mm. We considered the first slice in short axis at $z = 80$ mm and the last slice at $z = 20$ mm. Moreover the temporal resolution was set at 33.33 ms and phase number at 16, to achieve the maximum deformation at $t = 500$ ms.

The strain in the direction \mathbf{e} was calculated in the radial-circumferential coordinate system using the following equation:

$$\epsilon = \|\mathbf{F} \cdot \mathbf{e}\| - 1 \quad (3)$$

where \mathbf{F} is deformation gradient tensor with respect to the undeformed state.

The image intensity modulation produced by the SPAMM tagging pulse sequence was reproduced using the method in [7] to produce two sets of images, the first one with horizontal tag lines and the second one with vertical tag lines. Simulated images parameters were defined: FOV was 100×100 mm², the image matrix was 256×256 , the tag line distance was 5 mm and the tag line fading parameters was variable from 1 at undeformed state to 0.7 at maximum state of deformation. An example of synthetic images is shown in Fig. 1. In particular the first (Fig. 1.a) and the last frames (Fig. 1.b) of the first slice and a schematic representation of the respective Fourier transforms (Fig. 1.c and Fig. 1.d) are presented to show the peak displacement during the deformation.

2.2. Filter constraints

An important step in HARP analysis is the choice of the optimal elliptic filter parameters. As in [3], we decided to model the filter bandpass region with an ellipse because of its simple geometry that adequately include most of the spectral peaks. In particular, the cut-off frequencies are important to include all information about the deformation and to limit the errors.

We perform a simulation on the developed software model to investigate the effect of filter design on circumferential strain results obtained using HARP analysis. We defined an elliptical filter centered on the peak corresponding to the undeformed image and we fixed the ellipse principal axis (PA) in the displacement direction and the transversal axis (TA) in orthogonal direction. We simulated the effect of PA and TA parameters by evaluating the percentage errors between the estimated and the true value of the circumferential strain calculated at the mean radius and in the last frame. The results of the simulation for PA and TA ranging from 8 to 40 pixels are shown in Fig. 2.a. Since no information is included in the filter for axes size less than 8 ppx, we do not include them in the simulation. From the Fig. 2.a we can observe two main undesired situations that produce a large error in the strain evaluation. In the first case the PA size is smaller than peaks displacement and the information about last frame is not included in the elliptic filter (Fig. 2.c). In the latter case, the TA size is big enough to overlap with the central peak (Fig. 2.b). In this case a null strain is calculated and an error of 100% occurred.

The acceptable percentage error range is shown in Fig. 2.d corresponding to PA ranging from 26 to 40 and TA from 5 to 14. In this range, the better result is obtained for $PA = 35$ and $TA = 9$ where an error of 0.04% occurred and the worst result for $PA = 26$ and $TA = 13$ where the error is 15.3%. Indeed the range limits are the critical points because the percentage error grows up very quickly. For example, for $PA = 35$ and $TA = 14$ the percentage error is 4.24%, for $PA = 35$ and $TA = 15$ the percentage error is 52.33% and the error diverges to value $> 200\%$ for $PA = 35$ and $TA = 16$ because some information about central peak is included in the filter. On the basis of these results, we can appreciate the importance of filter design to ensure an acceptable error in the estimation of the mechanical variables.

2.3. Automatic filter design

We developed an automatic method to define the filter parameters. This method uses the Fourier transform images of every slice and frame in order to extract the information about a spectral peak. This method is applied to both tag lines orientation to obtain two filters. We model each peak in the Fourier spectrum with a bidimensional Gaussian function translated and rotated with respect to the image reference frame:

$$f(x', y') = \frac{1}{2\pi\sigma_{x'}\sigma_{y'}} e^{-\frac{(x'-\mu_{x'})^2}{2\sigma_{x'}^2}} e^{-\frac{(y'-\mu_{y'})^2}{2\sigma_{y'}^2}} \quad (4)$$

In this expression x' and y' represent the coordinates with respect to the local reference frame defined by:

$$\begin{pmatrix} x' \\ y' \end{pmatrix} = \begin{pmatrix} \cos\theta & -\sin\theta \\ \sin\theta & \cos\theta \end{pmatrix} \begin{pmatrix} x - \mu_x \\ y - \mu_y \end{pmatrix} \quad (5)$$

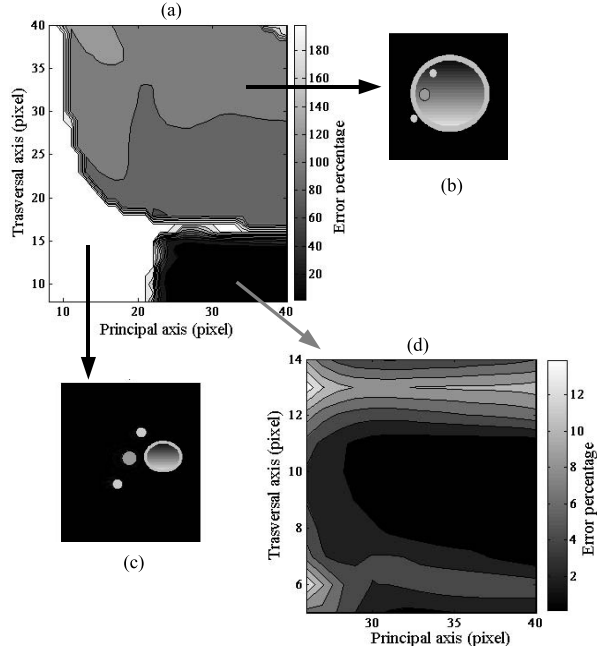


Fig. 2. Representation of the percentage error variability depending on the filter size.

where θ is the angle rotation of the local reference frame and $\boldsymbol{\mu} = [\mu_x; \mu_y]$ is the center of the bidimensional Gaussian function. In the Eq. 4, $\sigma_{x'}$ and $\sigma_{y'}$ represent the standard deviation values in the two orthogonal directions.

We use the nonlinear least squares fitting to determine the vector parameters $\boldsymbol{\lambda} = [\sigma_{x'}; \sigma_{y'}; \theta]$ of each bidimensional Gaussian function. In the fitting analysis, the vector parameters has been initialized at $\boldsymbol{\lambda}_0 = [1; 1; 0]$ and the nonlinear least square method is applied to an adaptive number of points around the peak center depending on the current $\sigma_{x'}$ and $\sigma_{y'}$ values. The automatic filter design method uses the following steps to define the optimal elliptical filter parameters:

1. the center of the central peak is set at the position of the maximum value of the first Fourier transform image;
2. we model the central peak using the first frame image. The bidimensional Gaussian parameters $\boldsymbol{\lambda}_0 = [\sigma_{0x'}; \sigma_{0y'}; \theta_0]$ are determined using the method described above. The central peak is modelled on the image plane using an ellipse centered in $\boldsymbol{\mu} = [\mu_x; \mu_y]$ (computed at step 1) and rotated of θ_0 angle. The ellipse axes size are defined as $\boldsymbol{r} = [4\sigma_{x'}; 4\sigma_{y'}]$ in order to include most of central peak;
3. in all Fourier transform images, the pixel values included in the central ellipse are set to zero. We place the center of each peak to the position of the maximum Fourier transform images value;
4. we model each lateral peak with a bidimensional

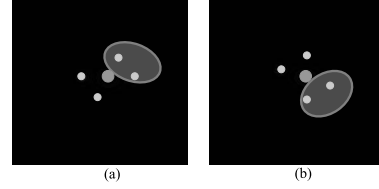


Fig. 3. Filter position for vertical (a) and horizontal (b) tag lines.

Gaussian function and we find the vector parameters $\boldsymbol{\lambda} = [\sigma_{p_{x'}}; \sigma_{p_{y'}}; \theta_p]$. Each peak is modelled on the image plane using an ellipse centered in $\boldsymbol{\mu}_p = [\mu_{x_p}; \mu_{y_p}]$ (computed at step 3) and rotated of θ_p angle. The ellipse axes size are defined as $\boldsymbol{r} = [f \cdot \sigma_{x'}; f \cdot \sigma_{y'}]$, where the initial value of f parameter is 7 and the optimal value is defined using an iterative algorithm described in detail in the following step;

5. we build an ellipse with minimum area that includes all lateral ellipses. In order to find the optimal f value (introduced in the previous step), we check if the total ellipse overlaps the central peak. We perform this control because, as demonstrated in Sec. 2.2, a large error occurs when the central peak is included in the filter. This check can produce two results:

- (a) *overlap*: we decrease the value of the factor f and we return to the step 4;
- (b) *non-overlap*: we accepted the found f value and we use the total ellipse to define the elliptical filter parameters $\boldsymbol{p} = [center_x; center_y; r_{x'}; r_{y'}; \theta]$. The iterative algorithm is stopped.

We applied the automatic method to the simulated images, with both horizontal and vertical tag lines. We obtained the filters shown in Fig. 3. In both cases the filter does not overlap with the central peak. In the elliptical filter, the standard deviation of Gaussian rolloff outside is set to $\sigma = 0.05$ [3].

3. RESULTS

The designed filter is used in HARP analysis to calculate the circumferential strain measured at the mean radius of the simulated images. Fig. 4 depicts the true circumferential strain and the results obtained using the designed filter in HARP analysis. The different curves, each corresponding to a different slice, show the same trend during the deformation. Notably we can observe that they are very close to the ‘true’ values.

We evaluated the developed method using real data from a normal pig heart by comparing the results obtained using manual definition of filter cut-off frequencies and the automatic method. MR-Tagging images was acquired on a GE

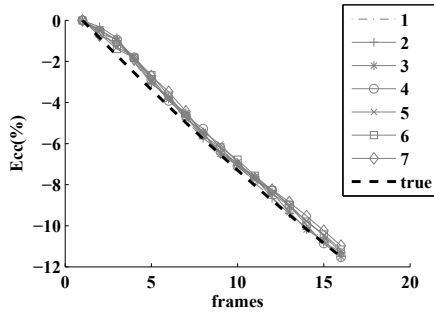


Fig. 4. Comparison between true and calculated circumferential strain in simulated data.

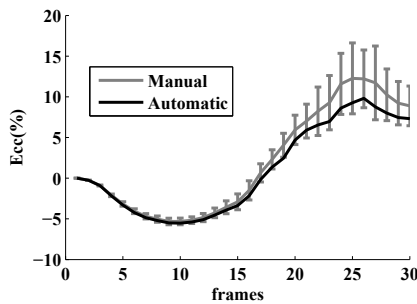


Fig. 5. Comparison between circumferential strain on real data obtained using manual and automatic filter definition method.

1.5T scanner with a Fast Gradient Echo (FGRE) pulse sequence (TR = 8.0 ms; TE = 4.4 ms; slice thickness 8 mm with no interslice gap; FOV 380 x 380; matrix size 256 x 256; view per segment 4; flip angle 12°; NEX = 3). The tagging pulse consisted of nonselective radio-frequency pulses separated by spatial modulation of magnetization (SPAMM) encoding gradients to achieve a parallel stripe tag pattern with a tag spacing of 5 pixels. Two sets of short axis images was acquired with the tag orientation of 45° and 135°.

Five independent operators utilized a manual definition of the filter cut-off frequencies in HARP analysis to calculate the circumferential strain. The same data have been also analyzed by using the automatic filter design technique proposed in this paper. In order to compare the results obtained by the two methods, the same mesh of endocardium, epicardium and midwall of the left ventricle was applied during the analysis. The segmental circumferential strain was estimated at midwall, and the mean value across six segments was calculated, thus obtaining a single value for each frame.

To analyze the inter-operator variability, we calculated the mean value and the standard deviation of the real data obtained using the manual method. The results are shown in Fig. 5 where the circumferential strain determined by automatic filter definition is also depicted. Again, the curves exhibit the same trend but the variability inter-operator caused by filtering step is suppressed using the automatic method.

4. CONCLUSION

In this paper we presented an automatic method to define the parameters of the bandpass filter used in HARP analysis. This method allows to include in the filtering step all spectral peaks that carry information about the deformation and to avoid a large error in strain evaluation. Moreover the automatic method eliminates the inter-operator variability caused by differences in the choice of the cut-off frequencies and thus in the definition of the filter size. Further work will include comparison of the method performance with respect to the other automated and semi-automated HARP methods.

5. REFERENCES

- [1] L. Axel, A. Montillo, and D. Kim, "Tagged magnetic resonance imaging of the heart: a survey," *Med Image Anal*, vol. 9, no. 4, pp. 376–393, August 2005.
- [2] N.F. Osman, W.S. Kerwin, E.R. McVeigh, and J.L. Prince, "Cardiac motion tracking using cine harmonic phase (harp) magnetic resonance imaging," *Magn Reson Med*, vol. 42, no. 6, pp. 1048–1060, December 1999.
- [3] N.F. Osman, E.R. McVeigh, and J.L. Prince, "Imaging heart motion using harmonic phase mri," *IEEE Trans Med Imaging*, vol. 19, no. 3, pp. 186–202, March 2000.
- [4] N.F. Osman and J.L. Prince, "Angle images for measuring heart motion from tagged mri," in *International Conference on Image Processing*, 4-7 October 1998, vol. 1, pp. 704–708.
- [5] N.F. Osman and J.L. Prince, "On the design of the band-pass filters in harmonic phase mri," in *International Conference on Image Processing*, 10-13 September 2000, vol. 1, pp. 625–628.
- [6] C.A. Davis, J. Li, and T.S.Jr. Denney, "Analysis of spectral changes and filter design in tagged cardiac mri," in *3rd IEEE International Symposium on Biomedical Imaging: Macro to Nano*, 6-9 April 2006, pp. 137–140.
- [7] J.P. Kuijjer, E. Jansen, J.T. Marcus, A.C. van Rossum, and R.M. Heethaar, "Improved harmonic phase myocardial strain maps.," *Magn Reson Med*, vol. 46, no. 5, pp. 993–999, November 2001.
- [8] A.A. Young and L. Axel, "Three-dimensional motion and deformation of the heart wall: estimation with spatial modulation of magnetization—a model-based approach," *Radiology*, vol. 185, no. 1, pp. 241–247, October 1992.
- [9] S.R.R. Tecelao, J.J.M. Zwanenburg, J.P.A. Kuijjer, and J.T. Marcus, "Extended harmonic phase tracking of myocardial motion: improved coverage of myocardium and its effect on strain results," *J Magn Reson Imaging*, vol. 23, no. 5, pp. 682–690, May 2006.